Saddle-point states and energy barriers for vortex entrance and exit in superconducting disks and rings

B. J. Baelus, F. M. Peeters,* and V. A. Schweigert†
Departement Natuurkunde, Universiteit Antwerpen (UIA), Universiteitsplein 1, B-2610 Antwerpen, Belgium
(Received 13 October 2000; published 21 March 2001)

The transitions between the different vortex states of thin mesoscopic superconducting disks and rings are studied using the nonlinear Ginzburg-Landau functional. They are saddle points of the free energy representing the energy barrier which has to be overcome for transition between the different vortex states. In small superconducting disks and rings the saddle point state between two giant vortex states, and in larger systems the saddle point state between a multivortex state and a giant vortex state and between two multivortex states is obtained. The shape and the height of the nucleation barrier is investigated for different disk and ring configurations.

DOI: 10.1103/PhysRevB.63.144517 PACS number(s): 74.60.Ec, 74.20.De, 73.23.−b

I. INTRODUCTION

The study of superconducting samples with sizes comparable to the penetration depth (λ) and the coherence length (ξ) became possible due to recent progress in nanofabrication technologies. This evolution resulted in an increase of interest in the investigation of flux penetration and flux expulsion in such mesoscopic samples in order to explain the hysteresis behavior and the different phase transitions in thin superconducting samples.[1–15]

It is well known that for type-II ($\kappa=\lambda/\xi>1/\sqrt{2}$) superconductors the triangular Abrikosov vortex lattice is energetically favored in the magnetic field range $H_{c1}<H<H_{c2}$ where κ is the Ginzburg-Landau (GL) parameter, and H_{c1} and H_{c2} are the first and second critical fields of a type-II superconductor. Since the effective London penetration depth $\Lambda=\lambda^2/d$ increases considerably in thin films one expects the appearance of the Abrikosov multivortex state even in thin type-I ($\kappa<1/\sqrt{2}$) superconductors when the thickness $d\ll\lambda$. But, in small confined systems there is a competition between the boundary of the sample, which tries to impose the symmetry of the sample boundary on the vortex configuration, and this triangular Abrikosov state. As a consequence, the effective GL parameter $\kappa^*=\Lambda/\xi$ is no longer the only controlling parameter which determines the shape of the vortex configuration in thin mesocopic superconducting samples.[6] Previous theoretical and experimental studies of superconducting disks and rings[1–16] found that, as a function of the applied field, there are transitions between circular symmetric vortex states (called giant vortex states) with different vorticity L. Experimentally it was found that the magnetic field at which the transition $L\rightarrow L+1$ occurs does not necessarily coincides with the magnetic field H_{tr} where the vorticity of the ground state changes from L to $L+1$, i.e., it is possible to drive the system in a metastable state. This is typical for first order phase transitions. For increasing applied field, the state with vorticity L remains stable up to the penetration field $H_p>H_{tr}$ and transits then to the superconducting state with vorticity $L+1$. For decreasing applied field, the state with vorticity $L+1$ remains stable down to the expulsion field $H_e<H_{tr}$ before going to the state with vorticity L. This hysteresis effect is a consequence of the presence of an energy barrier between the states with vorticity L and $L+1$. The latter corresponds to different minima of the free energy in configurational space and the lowest barrier between those two minima is a saddle point. This barrier arises from the fact that the superconducting current around a vortex is in the opposite direction to the screening currents at the surface of the sample.[17] This Bean-Livingston model has been refined to different sample geometries.[18–23] The time of flux penetration and expulsion is determined by the height of the energy barrier.

The experimental consequences of the existence of these metastable states are (i) hysteretic behavior,[2] (ii) paramagnetic Meissner effect,[24–29] (iii) fractional flux penetration,[30] and (iv) negative flux entrance,[30] i.e., a decrease of the flux penetration through the superconducting disk with increasing vorticity and increasing magnetic field.

Schweigert and Peeters[31] studied flux penetration and expulsion in thin superconducting disks and presented an approach to find the saddle point states. They calculated the height of the free energy barriers which separate the stable states with different vorticity L. We will extend their approach and present a systematic study of flux penetration and expulsion in thin superconducting disks and disks with a hole in the center, i.e., mesoscopic ring structures.

Bezryadin *et al.*[32] used the nonlinear GL equation to study the phase diagram of a thin-wire loop and a thin film with a circular hole in the limit $\kappa^*\gg 1$. They performed a stability analysis of the giant vortex state with vorticity L by allowing only the admixture of the $L+1$ vortex state. A more rigorous stability analysis was performed by Horane *et al.*[33] who studied the saddle points between two vortex states of a one dimensional wire of zero width. They allowed for more possible nonuniform perturbations which may make the vortex state unstable. They found that the transition between two angular momentum states occurs through a saddle point which has a zero in the order parameter at some point along the ring. Such a zero creates a phase slip center, allowing the phase winding required for the transition. Our systems have a nonzero radial width and consequently such a scenario is not possible because the order parameter is not allowed to be zero along a radial line. In fact it was found in

Ref. 31 that for a disk geometry, the saddle point for flux penetration corresponds to a state with suppressed superconductivity at the disk edge which acts as a nucleus for the following vortex creation. In the present paper we will find that for rings with a finite width this picture has to be modified because of the presence of two boundaries, i.e., two edges.

Recently, Palacios[26] calculated saddle point states and the energy barriers responsible for the metastabilities of superconducting mesoscopic disks using the lowest Landau level approximation. The central idea of his method was to find generic stationary solutions of the Ginzburg-Landau functional and to project the order parameter onto smaller subspaces spanned by a finite number l of eigenfunctions $\{L_1, L_2, \ldots, L_l\}$, where $0 \leqslant L_1 \leqslant L_2 \leqslant \cdots \leqslant L_l$. Palacios restricted himself to $l \leqslant 3$ and therefore his approach is a special case of the one of Ref. 31 where no such restriction on l was imposed and where also different radial states were included. Yampolskii and Peeters[34] investigated the influence of the boundary condition (surface enhancement) on the superconducting states and the energy barriers between those vortex states. They also restricted their calculations to $l \leqslant 3$.

Recently, Akkermans *et al.*[25] studied the behavior of metastable vortex states in infinite superconducting cylinders for $\kappa \gg 1$, i.e., the London regime. They considered the situation where the vortices are symmetrically distributed along a closed ring and they found structural phase transitions of vortex patterns between the metastable states. The key concept was the introduction of a special curve Γ, which embodies the main geometric features of a vortex configuration. This curve appears mathematically as a limit cycle of the system of currents generated by the vortex pattern and separates the paramagnetic and diamagnetic domains.

The paper is organized as follows. In Sec. II we present the theoretical model and the calculation method to obtain the saddle points. In Sec. III we study thin superconducting disks and extend and supplement our previous results.[31] We make a distinction between small and large superconducting disks. In small disks only the giant vortex state appears, while in larger disks multivortices can nucleate and transitions between different multivortices are possible.[35,36] In Sec. IV we consider superconducting rings, where we make a distinction between small and large rings. Our results are summarized in Sec. V.

II. THEORETICAL FORMALISM

In the present paper we consider very thin superconducting disks with radius R and thickness d, and superconducting rings with inner radius R_i and outer radius R_0. These mesoscopic superconducting systems are immersed in an insulating medium in the presence of a perpendicular uniform magnetic field H_0. To solve this problem, we follow the numerical approach of Schweigert and Peeters.[31] For very thin disks and rings, i.e., $Wd \ll \lambda^2$, with $W=R$ the radius of the disk or $W=R_0-R_i$ the width of the ring, the demagnetization effects can be neglected and the Ginzburg-Landau functional can be written as

$$G = G_n + \int d\vec{r}\left(\alpha|\Psi|^2 + \frac{\beta}{2}|\Psi|^4 + \Psi^* \hat{L} \Psi \right), \tag{1}$$

where G, G_n are the free energies of the superconducting and the normal states, Ψ is the complex order parameter, α and β are the GL coefficients which depend on the sample temperature. $\hat{L}$ is the kinetic energy operator for Cooper-pairs of charge $e^*=2e$ and mass $m^*=2m$, i.e.,

$$\hat{L} = (-i\hbar\vec{\nabla} - e^*\vec{A}/c)/2m^*, \tag{2}$$

where $\vec{A} = \vec{e}_\phi H_0 \rho/2$ is the vector potential of the uniform magnetic field H_0 written in cylindrical coordinates ρ and ϕ.

By expanding the order parameter $\Psi = \Sigma_i^N C_i \varphi_i$ in the orthonormal eigenfunctions of the kinetic energy operator $\hat{L}\varphi_i = \epsilon_i \varphi_i$,[5–7] the difference between the superconducting and the normal state Gibbs free energy can be written in terms of complex variables as

$$F = G - G_n = (\alpha + \epsilon_i) C_i C_i^* + \frac{\beta}{2} A_{kl}^{ij} C_i^* C_j^* C_k C_l, \tag{3}$$

where the matrix elements $A_{kl}^{ij} = \int d\vec{r} \varphi_i^* \varphi_j^* \varphi_k \varphi_l$ are calculated numerically. The boundary condition for these φ_i, corresponding to zero current density in the insulator media, is

$$\left(-i\hbar\vec{\nabla} - \frac{e^*\vec{A}}{c} \right)\Bigg|_n \varphi_i = 0. \tag{4}$$

These eigenenergies ϵ_i and the eigenfunctions φ_i depend on the sample geometry. For thin axial symmetric samples the eigenfunctions have the form $\varphi_{j=(n,l)}(\rho,\phi) = \exp(il\phi) f_n(\rho)$, where l is the angular momentum and the index n counts different states with the same l and equals the number of nodes in the radial direction. Thus, the order parameter Ψ can be written as

$$\psi = \sum_n \sum_l C_{n,l} \varphi_{n,l}. \tag{5}$$

We do not restrict ourselves to the lowest landau level approximation (i.e., $n=1$) and expand the order parameter over all eigenfunctions with energy $\epsilon_i < \epsilon_*$, where the cutting parameter ϵ_* is chosen such that increasing it does not influence the results. The typical number of complex components used are in the range $N=30-50$. Thus the superconducting state is mapped into a 2D cluster of N particles with coordinates $(x_i, y_i) \leftrightarrow [\mathrm{Re}(C_i), \mathrm{Im}(C_i)]$, whose energy is determined by the Hamiltonian (3). The energy landscape in this $(2N+1)$-dimensional space is studied where the local minima and the saddle points between them will be determined together with the corresponding vortex states.

To find the superconducting states and the saddle point states we use the technique described in Ref. 31. A particular state is given by its set of coefficients $\{C_i\}$. We calculate the free energy in the vicinity of this point $\delta G = G(C^n) - G(C)$ where $\{C^n\}$ is the set of coefficients of a state very close to the initial one. This free energy is expanded to second order in the deviations $\delta = C^n - C$,

$$\delta G = F_m \delta_m^* + B_{mn} \delta_n \delta_m^* + D_{mn} \delta_n^* \delta_m^* + \text{c.c.}, \tag{6}$$

where

$$F_m = (\alpha + \epsilon_i) C_m + \beta A_{kl}^{mj} C_j C_k^* C_l, \tag{7a}$$

$$B_{mn} = (\alpha + \epsilon_m) I_{mn} + 2\beta A_{kl}^{mn} C_k C_l^*, \tag{7b}$$

$$D_{mn} = \beta A_{kl}^{mn} C_k C_l, \tag{7c}$$

and I_{mn} is the unit matrix. Using normal coordinates $\delta_m = x_k Q_m^k$ we can rewrite the quadratic form as $\delta G = 2(\gamma_k x_k + \eta_k x_k^2)$. To find the eigenvalues η_k and the eigenvectors γ_k we solve numerically the following equation:

$$\begin{vmatrix} B + \mathrm{Re}(D) & \mathrm{Im}(D) \\ \mathrm{Im}(D) & B - \mathrm{Re}(D) \end{vmatrix} \begin{vmatrix} \mathrm{Re}(Q^k) \\ \mathrm{Im}(Q^k) \end{vmatrix} = \eta_k \begin{vmatrix} \mathrm{Re}(Q^k) \\ \mathrm{Im}(Q^k) \end{vmatrix}. \tag{8}$$

Starting from a randomly choosen initial set of coefficients, we calculate a nearby minimum of the free energy by moving in the direction of the negative free energy gradient $-\gamma_k$. The set of coefficients of this minimum determines then the ground state or a metastable state. Starting from the initial set of coefficients we can also calculate a nearby saddle point state by moving to a minimum of the free energy in all directions, except the one which has the lowest eigenvalue. In this direction we move to a local maximum. Repeating this procedure for many randomly choosen initial sets of coefficients $\{C_i\}$ for fixed magnetic field, we find the different possible superconducting states and saddle point states. To calculate the magnetic field dependence we start from a superconducting state at a certain field and we change the applied field by small increments. By moving into the direction of the nearest minimum or saddle point, the corresponding state will be found for the new magnetic field, provided that the field step is small enough.

III. SUPERCONDUCTING DISKS

In the present section we discuss superconducting disks. Although the system is circular symmetric, in general we are not allowed to assume that $\Psi(\rho,\phi) = F(\rho) e^{iL\phi}$ because of the nonlinear term in the GL functional. Nevertheless, in small disks the confinement effects are dominant and this imposes a circular symmetry on the superconducting condensate, which means that only the ''giant'' vortex state, i.e., a circular symmetric vortex state, is realized. For larger disks and not too large magnetic fields, the confinement effects are no longer dominant and multivortices can nucleate in a certain magnetic field range. For this reason we make a distinction between small and large disks.

A. Small disks: Giant vortex state

We consider superconducting disks with radius $R = 2.0\xi$. First we investigate the influence of the number of terms in the expansion of Eq. (5) on the energy of the minima and the saddle points. For the approach that $n = 1$ (i.e., lowest Landau level) and if only one l is taken into account for each state, i.e., $\Psi = C_l \varphi_l$, we find three different states for three different values of l, $l = 0$, 1, and 2, in different magnetic field regions. In Fig. 1(a) the free energy F of these L states, measured in units of the condensation energy $F_0 = \alpha^2 \pi R^2 d/2\beta$, is shown by the dotted curves as a function of the applied magnetic field H_0. Next, we take into account two values of l and $n = 1$, i.e., $\Psi = C_{l_1} \varphi_{l_1} + C_{l_2} \varphi_{l_2}$ as was done in, e.g., Ref. 26. With this approach we find L states with $L = 0,1,2$ and because of the concomittant existence of two minima also saddle point states with $(l_1, l_2) = (0,1)$ and $(1,2)$ appear. These are the saddle point states for the transition between L states with $L = l_1$ and $L = l_2$. In Fig. 1(a) the L states for this approach are given by the solid curves and the saddle point states by the dashed curves. The inset shows the transition between the $L = 1$ state and the $L = 2$ state in more detail. Notice that including one extra term in Eq. (5) reduces appreciably the stability region of the different giant vortex states, i.e., its metastable region is strongly reduced. The L states are only stable up to the point where its energy equals the saddle point states.

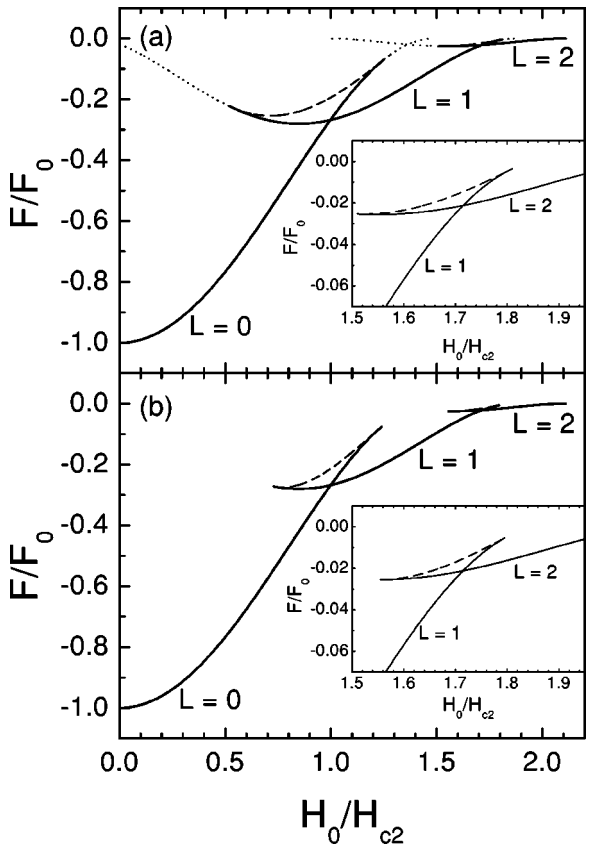

FIG. 1. The energy of the minima in the free energy F and the energy of the saddle points as a function of the applied magnetic field H_0 for a superconducting disk with radius $R = 2.0\xi$. (a) When only one term is included, i.e., $(n,l) = (1,l)$ (dotted curve), when two l values are included, i.e., (n,l_1) and (n,l_2) (solid curves), with the corresponding energy of the saddle point (dashed curves). (b) The giant vortex energy (solid curves) and the saddle point energy (dashed curves) when an arbitrary large number of terms are included. The free energy is scaled with the condensation energy $F_0 = \alpha^2 \pi R^2 d/2\beta$.

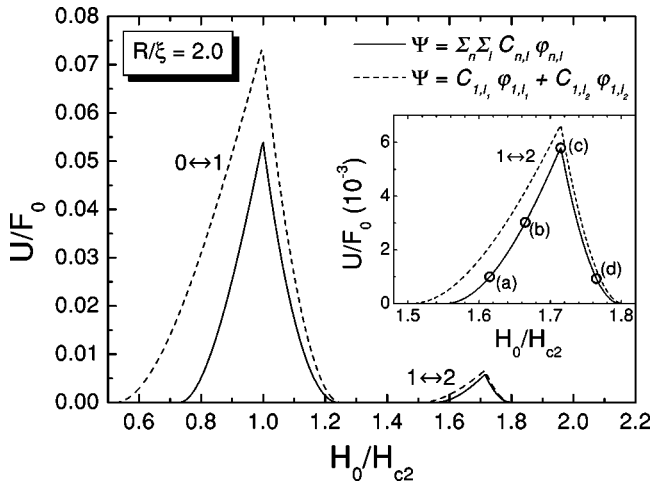

FIG. 2. The transition barrier U for transitions between different L-states for a superconducting disk with radius $R=2.0\xi$ when taking into account only two values of l (dashed curves) and for the numerical ''exact'' result (solid curves). The inset shows the second barrier in more detail.

Figure 1(b) shows the free energy as a function of the applied magnetic field if we do not restrict ourselves to the lowest landau level and if we expand the order parameter over all eigenfunctions with energy $\epsilon_i < \epsilon_*$, where the cutting parameter ϵ_* is chosen such that increasing it does not influence the results. The solid and the dashed curves indicate, respectively, the stable L states and the saddle point states. The transition between the $L=1$ state and the $L=2$ state is enlarged in the inset. Notice that the stability region of the L states is further reduced. Allowing more basis functions in Eq. (5) does not have a strong influence on the energy of the L states, e.g., compare the dotted and the solid curves in Fig. 1(a), but it considerably decreases the energy of the saddle point between the L states. In doing so, it reduces strongly the stability range of the metastable states, and consequently it reduces the size, i.e., the width in the magnetic field range, of the hysteresis effect.[23] For example, we found $(H_{tr}/H_{c2}, H_e/H_{c2}, H_p/H_{c2}) \approx (1.0, 0.52, 1.25)$, (1.0,0.715,1.245), and (1.0,0.73,1.24) for the $L=0 \leftrightarrow L=1$ transition when we include two, three, and an arbitrary number of basis function in Eq. (5), respectively. Similarly, we found for the $L=1 \leftrightarrow L=2$ transition $(H_{tr}/H_{c2}, H_e/H_{c2}, H_p/H_{c2}) \approx (1.715, 1.52, 1.81)$, (1.715,1.535,1.80), and (1.715,1.555,1.795) including two, three, and an arbitrary number of basis functions, respectively. These results clearly show that one has to exert some caution to cutoff the expansion in Eq. (5) when calculating the saddle point and thus the energy barriers. Notice that the expulsion field H_e/H_{c2} is most strongly influenced by the number of terms in Eq. (5).

In Fig. 2 the transition barriers U, i.e., the energy difference between the saddle point state and the nearby metastable states are plotted. We show the ''exact'' numerical results (solid curves) and the results when including only two values of l with $n=1$, i.e., $\Psi = C_{l_1}\varphi_{l_1} + C_{l_2}\varphi_{l_2}$ (dashed curves). Notice that by approximating the order parameter better: (i) it substantially lowers the energy barriers, (ii) it increases the expulsion fields H_e, and (iii) lowers the penetration fields H_p slightly. The energy barrier is smaller for higher $L \rightarrow L+1$ transitions which occur at larger magnetic fields. The inset shows the barrier between the $L=1$ and the $L=2$ state in more detail.

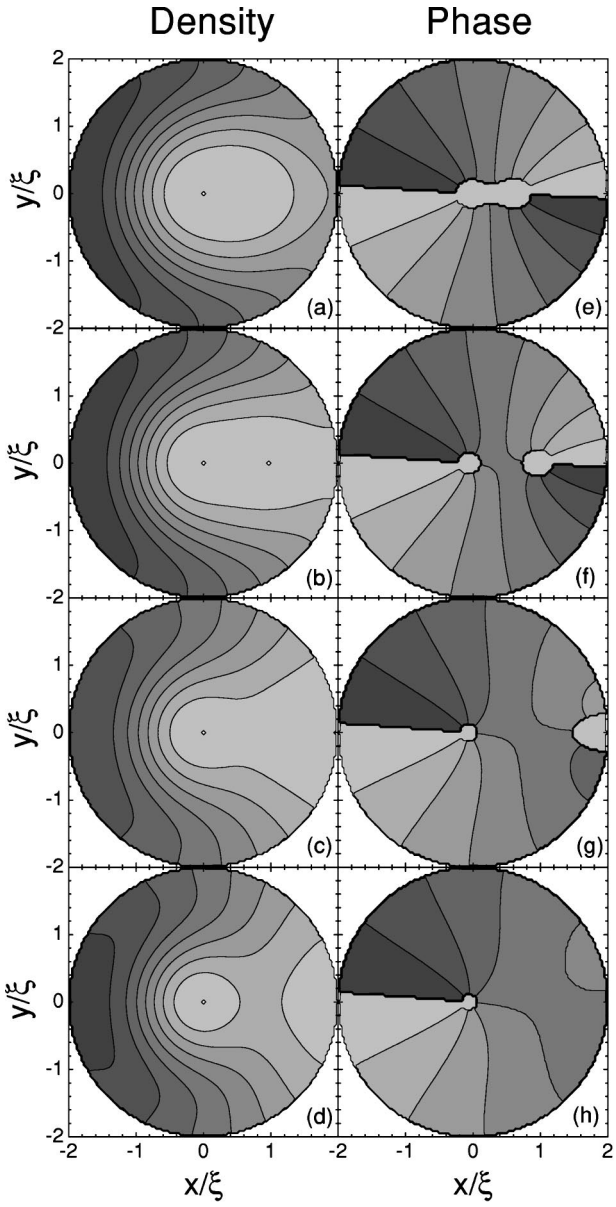

FIG. 3. The spatial distribution of the superconducting electron density $|\Psi|^2$ (a)–(d) and the phase of the order parameter (e)–(h) in the saddle point state corresponding to the transition from the $L=1$ state to the $L=2$ states in a superconducting disk with radius $R=2.0\xi$ for the magnetic fields indicated by the open circles in the inset of Fig. 2; $H_0/H_{c2}=1.615$ (a),(e), 1.665 (b),(f), 1.715 (i.e., the maximum of the barrier) (c),(g) and 1.765 (d),(h). High Cooper-pair density is given by dark regions, low Cooper-pair density by light regions. Phases $\varphi \gtrsim 0$ are given by light regions and $\varphi \lesssim 2\pi$ by dark regions.

The spatial distribution of the superconducting electron density $|\Psi|^2$ in the saddle point state corresponding to the transition from the $L=1$ state to the $L=2$ states is depicted in Figs. 3(a)–3(d) for the magnetic fields indicated by the open circles in the inset of Fig. 2, i.e., $H_0/H_{c2}=1.615$,

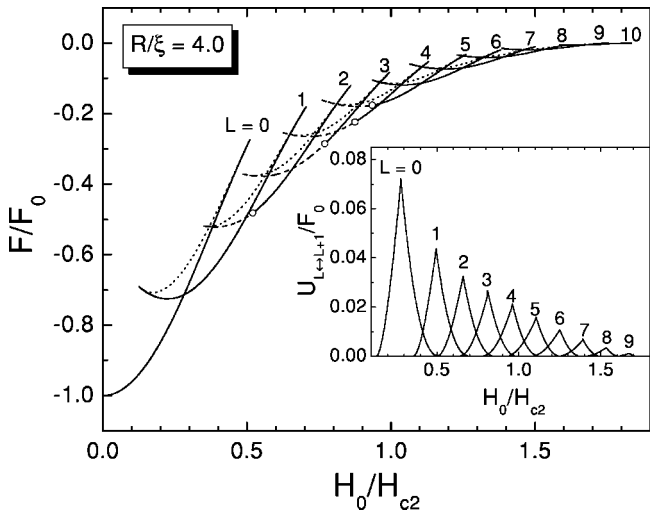

FIG. 4. The free energy as a function of the applied magnetic field H_0 for a disk with radius $R=4.0\xi$. The different L states are given by solid curves when in the giant vortex states and by dashed curves when in the multivortex states, while the saddle point states are given by the dotted curves. The open circles correspond to the transitions between the multivortex state and the giant vortex state for fixed L. The inset shows the transition barrier U as a function of the applied field for the different $L\leftrightarrow L+1$ transitions.

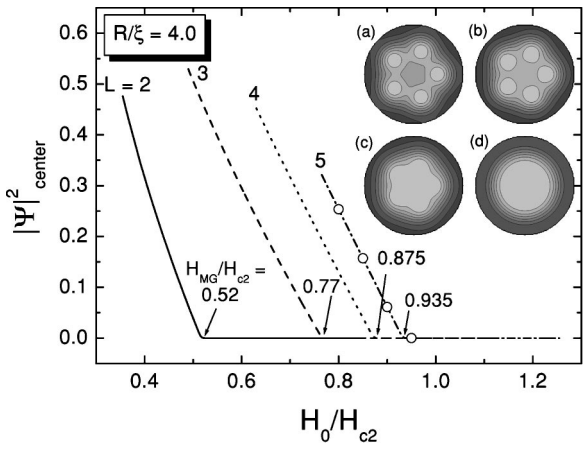

FIG. 5. The Cooper-pair density $|\Psi|^2$ in the center of the disk with radius $R=4.0\xi$ for $L=2$, 3, 4, and 5. The insets (a)–(d) show the spatial distribution of the superconducting electron density for $L=5$ at the magnetic fields corresponding to the open circles; i.e., $H_0/H_{c2}=0.8$, 0.85, 0.9, and 0.95, respectively. The transition from multivortex state to giant vortex state occurs at the transition field H_{MG}.

1.665, 1.715 (i.e., the maximum of the barrier) and 1.765, respectively. In Ref. 31 similar results were shown for the $L=0\leftrightarrow L=1$ saddle point. High (low) Cooper-pair density is given by dark (light) regions. The little white spots in the superconductor show the centers of the vortices. With increasing field, one vortex moves from the center to the outer region of the disk, and the state changes from $L=2$ to $L=1$. This is better illustrated by the contour plots of the phase of the order parameter which is shown in Figs. 3(e)–3(h) for the same configurations. Along a closed path, which lies near the edge of the superconductor, the phase difference $\Delta\varphi$ is always given by L times 2π, with L the vorticity or winding number. Light regions indicate phases $\varphi\gtrsim 0$ and dark regions $\varphi\lesssim 2\pi$. When encircling the superconductor near the boundary, we find that the phase difference $\Delta\varphi$ is equal to $2\times 2\pi$ in Figs. 3(e)–3(g) and $\Delta\varphi=1\times 2\pi$ in Fig. 3(h), which means vorticy $L=2$ and 1, respectively. At the maximum of the barrier, i.e., when the energy of state $L=1$ and $L=2$ are identical, the saddle point transits from vorticity $L=2$ to $L=1$. At this point the Cooper-pair density is zero at the boundary of the disk which acts as a nucleation center for flux penetration and expulsion.[31]

B. Large disks: Multivortex states

We consider now a larger superconducting disk with radius $R=4.0\xi$ in which multivortex states can nucleate in certain magnetic field ranges.[6,35] Figure 4 shows the free energy as a function of the applied magnetic field H_0. The energy of the different L states is given by solid curves when they are in the giant vortex state and by dashed curves when they are in the multivortex state and the saddle point states are given by the dotted curves. The open circles give the transition points between the multivortex state and the giant vortex state for fixed L. The inset shows the transition barrier U as a function of the applied field for the different $L\leftrightarrow L+1$ transitions. To distinguish qualitatively the giant vortex state from the multivortex state for fixed L we considered the value of the Cooper-pair density $|\Psi|^2$ in the center of the disk. Figure 5 shows $|\Psi|^2_{\text{center}}$ which is zero for a giant vortex state and nonzero in the multivortex states when there is no vortex in the center of the disk. For $R=4.0\xi$ we find only multivortex states for $L=2$, 3, 4, and 5 and the transition from the multivortex state to the giant vortex state occurs at $H_{MG}/H_{c2}=0.52$, 0.77, 0.875, and 0.935, respectively. Of course, for $L=1$ there is no distinction between the giant and the multivortex state. For $L=5$ the spatial distribution of the superconducting electron density is given in the insets (a)–(d) of Fig. 5 at the magnetic fields corresponding to the open circles in Fig. 5, i.e., $H_0/H_{c2}=0.8$, 0.85, 0.9, and 0.95, respectively. In the multivortex state the vortices move towards the center with increasing magnetic field and at the same time the vortices become wider, and therefore, the Cooper-pair density in the center decreases until the axial symmetry is recovered at the transition field $H_{MG}=0.935H_{c2}$.

Next, we will study the energy barriers U in more detail. For a superconducting disk with radius $R=4.0\xi$ the energy barriers for the different $L\leftrightarrow L+1$ transitions are shown in the inset of Fig. 4. The height of the energy barrier for the $L\leftrightarrow L+1$ transition decreases with increasing L. The difference between penetration and expulsion field decreases also with increasing L. Figure 6(a) shows the free energy of the $L=4$ and the $L=5$ states in more detail (solid curves for the giant vortex state and dashed curves for the multivortex state) together with the energy of the saddle point state between these states (dash-dotted curve). Figure 6(b) gives the corresponding energy barrier. The open circles correspond to the transition from multivortex to giant vortex state. The bar-

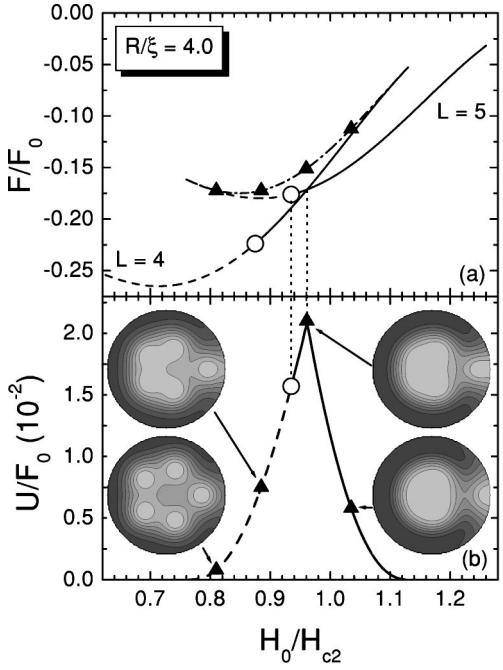

FIG. 6. (a) The free energy of the $L=4$ and the $L=5$ states (solid curves for giant vortex states and dashed curves for multivortex states) and the saddle point states between these states (dash-dotted curve) for a superconducting disk with radius $R=4.0\xi$; and (b) the energy barrier corresponding with this transition. The open circles correspond with the transition from multivortex to giant vortex state for fixed L. The insets show the spatial distribution of the superconducting electron density $|\Psi|^2$ for the saddle point states indicated by triangles, i.e., at the magnetic fields $H_0/H_{c2}=0.81$, 0.885, 0.96 (the barrier maximum), and 1.035. It is the transition between a multivortex state with $L=5$ and a giant vortex state with $L=4$.

rier height is clearly not influenced by the transition from multivortex to giant vortex state, i.e., there are no jumps or discontinuities at the transition. The spatial distribution of the superconducting electron density $|\Psi|^2$ for this saddle point state is depicted in the insets of Fig. 6(b) for the configurations indicated by the triangles, i.e., $H_0/H_{c2}=0.81$, 0.885, 0.96 (the barrier maximum), and 1.035, respectively. Notice that also in the saddle point the transition between a multivortex state with $L=5$ and a giant vortex state with $L=4$ is clearly visible.

Near the maximum of the barrier, the barrier height changes linearly with magnetic field. Therefore, we can approximate the energy barrier U near its maximum $U_{\max}$ by

$$\frac{U}{F_0}=\frac{U_{\max}}{F_0}+\alpha\frac{H-H_{\max}}{H_{c2}},$$

where the slope α is positive for $H\lesssim H_{\max}$ and negative for $H\gtrsim H_{\max}$. In Fig. 7 the absolute value of the slope $|\alpha|$ is given as a function of L for $H\lesssim H_{\max}$ by the closed circles and for $H\gtrsim H_{\max}$ by the open circles. The absolute value of the slope is different for the left and the right side of the maximum of the barrier. Notice that for $L=0$ and $L=1$, $|\alpha|$ is larger for $H\lesssim H_{\max}$ as compared to $H\gtrsim H_{\max}$, while for

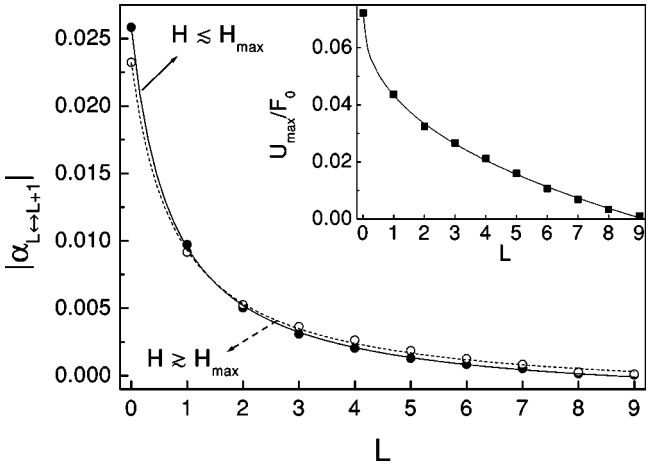

FIG. 7. The absolute value of the slope $|\alpha|$ of the energy barrier for a superconducting disk with $R=4.0\xi$ as a function of L for $H\lesssim H_{\max}$ (closed circles) and for $H\gtrsim H_{\max}$ (open circles). The inset shows the maximum barrier height as a function of the vorticity L. The solid and dashed curves are the results of a fit.

$L>1$ the reverse is true. For increasing L the slope decreases and the behavior could be fitted to

$$|\alpha_{L\leftrightarrow L+1}(L)|=\frac{a+bL}{1+cL},$$

with $a=0.02586$, $b=-0.00300$, and $c=1.40357$ for $H\lesssim H_{\max}$, and $a=0.02322$, $b=-0.00217$, and $c=1.26502$ for $H\gtrsim H_{\max}$. These fitting curves are shown in Fig. 7 by the solid line for $H\lesssim H_{\max}$ and by the dashed line for $H\gtrsim H_{\max}$. In the inset of Fig. 7 the maximum of the barrier height $U_{\max}$ is given by the symbols as a function of the vorticity L. The barrier height decreases for increasing vorticity and the behavior could be fitted to

$$\frac{U_{\max}}{F_0}(L)=\frac{a+bL}{1+c\sqrt{L}},$$

with $a=0.07229$, $b=-0.00791$, and $c=0.48657$, which is shown by the solid curve.

For larger superconducting disks and higher values of L, different configurations of multivortices can occur with the same vorticity.[25,27,36] Figure 8 shows the free energy as a function of the applied field for the superconducting states with vorticity $L=6$ and $L=7$. For both vorticities two configurations are possible; (i) L vortices on a ring and no vortex in the center (solid curve) and (ii) $L-1$ vortices on a ring and 1 in the center (dashed curve). The vortex state is completely determined by the number of vortices in the center L_{center} and the total number of vortices L. For this reason we characterized the states by the indices $(L_{\text{center}};L)$ in Fig. 8. The insets show the Cooper-pair density at $H_0/H_{c2}=0.6$ for the (0;6) state, the (1;6) state, the (0;7) state, and the (1;7) state, respectively. Notice further that for such large radius, there is no transition from a multivortex to a giant vortex state for these values of L. For the sake of clarity, only the free energy of the saddle point state between the (1;7)

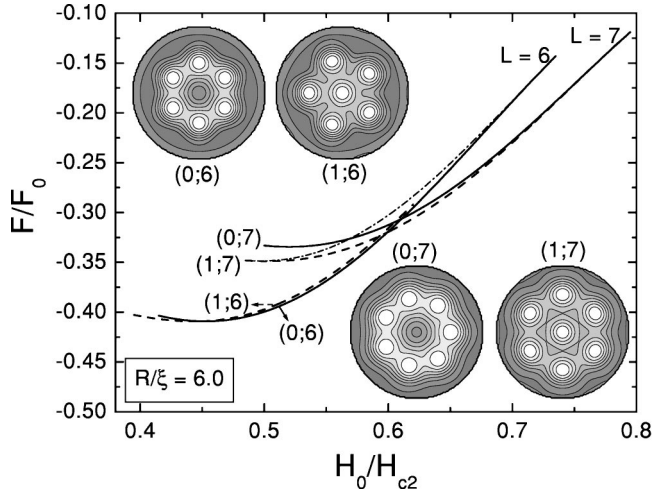

FIG. 8. The free energy F as a function of the applied magnetic field H_0 of the (0;6) and the (0;7) state (solid curves), the (1;6) and the (1;7) state (dashed curves), and the saddle point state (dash-dotted curve) between the (1;7) and (0;6) state for a superconducting disk with radius $R=6.0\xi$. The insets show the Cooper-pair density of the $(0;6)$ state, the (1;6) state, the (0;7) state, and the (1;7) state at the thermodynamic transition field $H_0/H_{c2}=0.6$ between the (0;6) and the (1;7) state.

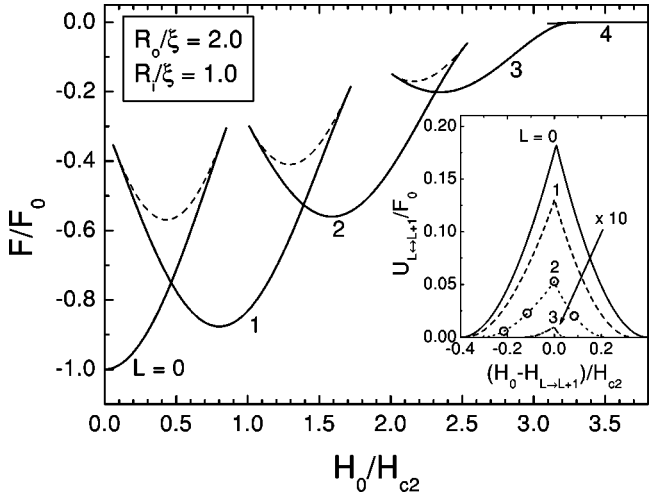

FIG. 10. The free energy for a superconducting ring with radius $R_0=2.0\xi$ and hole radius $R_i=1.0\xi$ as a function of the applied magnetic field for the different giant vortex states (solid curves) and for the saddle point states (dashed curves). The inset shows the energy barrier U for the transitions between different L states as a function of the difference between the applied magnetic field H_0 and the $L\rightarrow L+1$ transition field $H_{L\rightarrow L+1}$.

state and the $(0;6)$ state is given, as an example, by the dash-dotted curve in Fig. 8. This state describes the expulsion of one vortex when the system transits from the $L=7$ to the $L=6$ configuration and is illustrated in Figs. 9(a)–9(c) where we show the spatial distribution of the superconducting electron density $|\Psi|^2$ in the saddle point state at $H_0/H_{c2}=0.5$, 0.6, and 0.7, respectively. To transit from $L=7$ to $L=6$, one vortex on the ring moves towards the outside of the disk and the vortex in the center takes the free place on the ring. High (low) Cooper-pair density is given by dark (light) regions.

IV. SUPERCONDUCTING RINGS

Now, we will consider superconducting disks with radius R_0 with a hole in the center with radius R_i. For the same reason as in Sec. III we make a distinction between small and large systems.

A. Small rings: Giant vortex state

As an example, we consider a superconducting ring with radius $R_0=2.0\xi$ and hole radius $R_i=1.0\xi$. In Fig. 10 the free energy is shown as a function of the applied magnetic field for the different L states (solid curves) together with the saddle point states (dashed curves). We find giant vortex states with $L=0,1,2,3,4$. Comparing this result with the result for a disk with radius $R=2.0\xi$, more L states are possible and the superconducting/normal-transition moves to larger magnetic fields.[14] The inset shows the energy barrier U for the transitions between the different L states as a function of the difference between the applied magnetic field H_0 and the $L\rightarrow L+1$ transition field $H_{L\rightarrow L+1}$. For increasing L, the height of the energy barrier and the difference between the penetration and the expulsion field decreases. The energy barrier near its maximum can be approximated by $U/F_0=U_{\max}/F_0+\alpha(H-H_{\max})/H_{c2}$, and we determined the slope $\alpha_{L\rightarrow L+1}$; $\alpha_{0\rightarrow 1}=-0.8$ for $H\lesssim H_{\max}$ and 0.9 for $H\gtrsim H_{\max}$, $\alpha_{1\rightarrow 2}=-0.6$ for $H\lesssim H_{\max}$ and 0.75 for $H\gtrsim H_{\max}$, $\alpha_{2\rightarrow 3}=-0.3$ for $H\lesssim H_{\max}$ and 0.42 for $H\gtrsim H_{\max}$, and $\alpha_{3\rightarrow 4}=-0.013$ for $H\lesssim H_{\max}$, and 0.038 for $H\gtrsim H_{\max}$. The slope decreases again for increasing L and the absolute value of the slope for $H\lesssim H_{\max}$ is smaller than for $H\gtrsim H_{\max}$ for every L, although the difference is relatively smaller than in the previous disk case where we found $\alpha_{0\rightarrow 1}=-0.31$ for $H\lesssim H_{\max}$ and 0.44 for $H\gtrsim H_{\max}$, and $\alpha_{1\rightarrow 2}=-0.06$ for $H\lesssim H_{\max}$ and 0.1 for $H\gtrsim H_{\max}$.

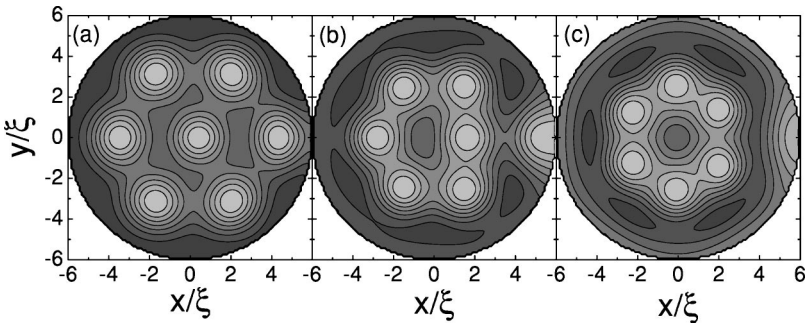

FIG. 9. The spatial distribution of the superconducting electron density $|\Psi|^2$ for the transition between the $L=6$ state and the $L=7$ state for a superconducting disk with radius $R/\xi=6.0$ at the applied magnetic fields $H_0/H_{c2}=0.5$ (a), 0.6 (b), and 0.7 (c).

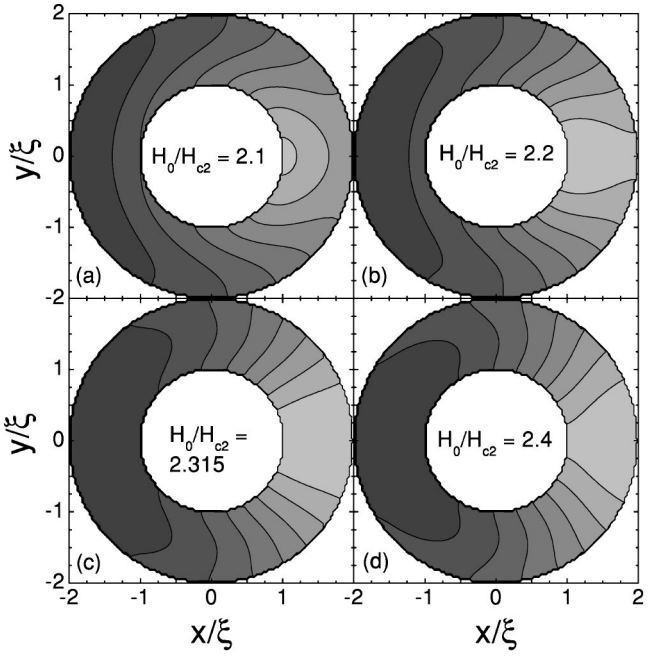

FIG. 11. The spatial distribution of the superconducting electron density $|\Psi|^2$ of the transition between the giant vortex states with $L=2$ and $L=3$ for a superconducting ring with $R_0=2.0\xi$ and $R_i=1.0\xi$ at $H_0/H_{c2}=2.1$ (a), 2.2 (b), 2.315 (c), and 2.4 (d). High density is given by dark regions and low density by light regions.

Next, we investigate the $2\leftrightarrow3$ saddle point. At $H_0/H_{c2}=2.01$ (expulsion field) and 2.535 (penetration field) the saddle point state equals the giant vortex states with $L=3$ and $L=2$, respectively. The transition between these two giant vortex states is illustrated in Figs. 11(a)–11(d) which show the spatial distribution of the superconducting electron density $|\Psi|^2$ corresponding with the open circles in the inset of Fig. 10 at $H_0/H_{c2}=2.1$, 2.2, 2.315 (i.e., the barrier maximum) and 2.4, respectively. High (low) density is given by dark (light) regions. With increasing field one vortex moves from inside the ring, through the superconducting material, to outside the ring. From Fig. 11(c) one may infer that the Cooper-pair density is zero along a radial line and that the vortex is, in fact, a sort of line. That this is not the case can be seen from the left inset of Fig. 12 which shows the Cooper-pair density $|\psi|^2$ along this radial line for $H_0/H_{c2}=2.315$. The Cooper-pair density in the superconducting material is zero only at the center of the vortex which is situated at $x_{\min}/\xi\approx1.5$ and $|\Psi|^2$ is very small otherwise, i.e., $|\Psi|^2<0.01$. In Fig. 12 the position of the vortex, i.e., of $x_{\min}$, is shown as a function of the applied field. Over a narrow field region the vortex moves from the inner boundary towards the outer boundary. From $H_0/H_{c2}=2.01$ to 2.25 the center of the vortex is still situated in the hole but the vortex already influences the superconducting state [see, for example, Figs. 11(a),11(b)]. From $H_0/H_{c2}=2.36$ to 2.535 the center of the vortex lies outside the ring, but it has still an influence on the saddle point [see, for example, Fig. 11(d)]. In the region $H_0/H_{c2}=2.25-2.36$ the center of the vortex is situated inside the superconductor. This is also illustrated by the contourplot (right inset of Fig. 12) for the phase of the order

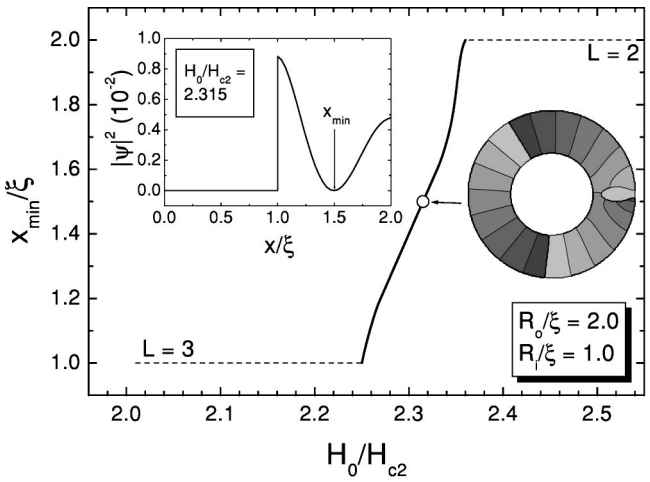

FIG. 12. The radial position of the vortex in the saddle point for the $2\leftrightarrow3$ transition through the superconductor with radius $R_0=2.0\xi$ and $R_i=1.0\xi$. The left inset shows the Cooper-pair density along the x direction at $H_0/H_{c2}=2.315$, and the right inset is a contour plot of the phase of the order parameter at $H_0/H_{c2}=2.315$.

parameter at $H_0/H_{c2}=2.315$, corresponding with the open circle in Fig. 12. When encircling the superconductor near the inner boundary of the ring, we find that the phase difference $\Delta\varphi$ is equal to $2\times2\pi$ which implies vorticity $L=2$. When encircling the superconductor near the outer boundary, we find vorticity $L=3$. If we choose a path around the vortex (located at $x_{\min}$), the phase changes with 2π and thus $L=1$. At the transition field ($H_0/H_{c2}=2.315$) the center of the vortex of the saddle point is clearly not situated at the outer boundary as was the case for superconducting disks [see, for example, Figs. 3(c), 3(g), 6(b), 9(b), and Ref. 31].

To illustrate this more clearly, Figs. 13(a),13(b) show the radial position of the vortex during the transition between the Meissner state and the $L=1$ state, and between the $L=1$ state and the $L=2$ state for a superconducting ring with ra-

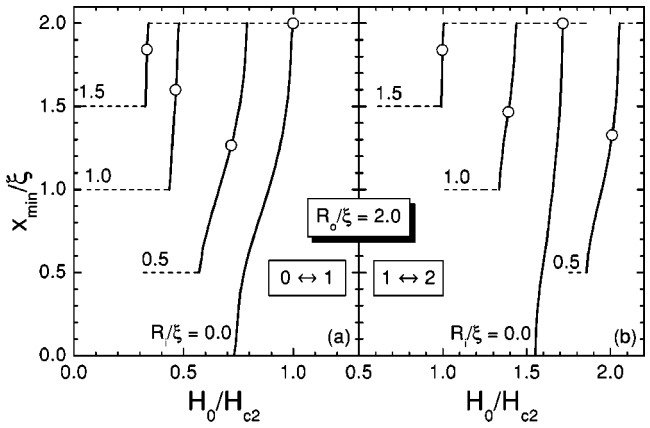

FIG. 13. The radial position of the vortex for (a) the $0\leftrightarrow1$ and (b) the $1\leftrightarrow2$ saddle point transition as a function of the applied magnetic field for a superconducting ring with radius $R_0=2.0\xi$ and $R_i=0.0$, 0.5, 1.0, and 1.5ξ. The open circles indicate the transition fields.

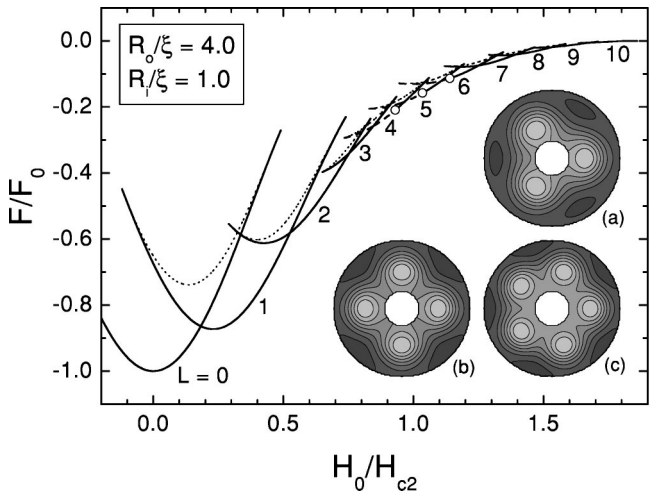

FIG. 14. The free energy for a superconducting ring with $R_0 = 4.0\xi$ and $R_i = 1.0\xi$ as a function of the applied magnetic field for the different L states (solid curves for giant vortex states and dashed curves for multivortex states), and the saddle point states (dotted curves). The open circles correspond to the transition between the multivortex state and the giant vortex state for fixed L. The inset shows the spatial distribution of the superconducting electron density $|\Psi|^2$ for the multivortex state with $L=4$ at $H_0/H_{c2}=0.8$ (a), $L=5$ at $H_0/H_{c2}=0.9$ (b) and $L=6$ at $H_0/H_{c2}=1.0$ (c). High Cooper-pair density is given by dark regions, low Cooper-pair density by light regions.

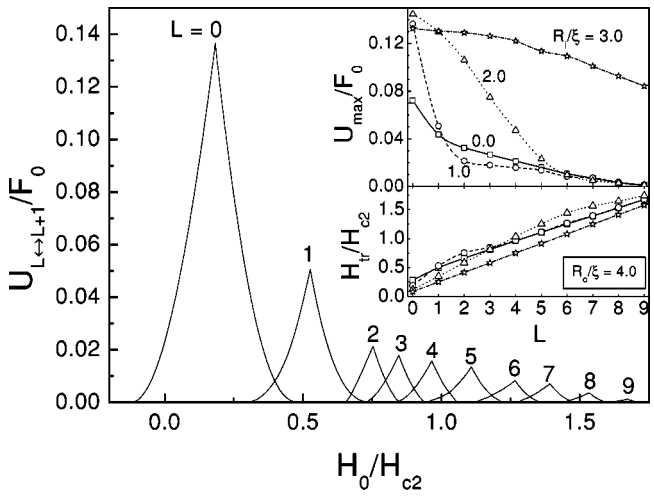

FIG. 15. The energy barrier U for the transitions between the different L states in a superconducting ring with $R_0=4.0\xi$ and $R_i = 1.0\xi$ as a function of the applied magnetic field. The insets show the maximum height of the energy barrier $U_{\max}$ and the transition field H_{tr} as a function of L for rings with $R_0=4.0\xi$ and $R_i=0.0$, 1.0, 2.0, and 3.0ξ.

dius $R_0=2.0\xi$ and for several values of the hole radius, i.e., $R_i/\xi=0.0$, 0.5, 1.0, and 1.5. The open circles indicate the ground state transition fields. Only for the case of the disk without a hole the center of the vortex at the saddle point occurs at the outer boundary of the disk for the magnetic field at which the ground state changes from L to $L+1$. When the disk contains a hole in the center there are two boundaries and the center of the above vortex is now located between those two boundaries. For a small hole with radius $R_i=0.5\xi$ the position of the vortex can be approximated by the arithmetic mean of the inner and the outer radius, i.e., $x_{\min}/\xi \approx (R_0+R_i)/2$, and for a larger hole with radius $R_i = 1.5\xi$ by the geometric mean $\sqrt{R_0 R_i}$. The transition field increases and the magnetic field range, over which the transition occurs, decreases with increasing L. Notice that the transition field for the $L=1\leftrightarrow 2$ transition for $R_i/\xi=0.5$ is larger than the one for $R_i/\xi=0.0$ [see Fig. 13(b)], which agrees with Fig. 4 of Ref. 14.

B. Large rings: Multivortex states

First, we consider superconducting rings with radius $R_0 = 4.0\xi$ and hole radius $R_i=1.0\xi$. In Fig. 14 the free energy is shown as a function of the applied magnetic field. The different L states are given by solid curves for giant vortex states and dashed curves for multivortex states, while the saddle point states are given by the dotted curves. The open circles correspond to the transition between the multivortex state and the giant vortex state for fixed L. These transitions occur at $H_{MG}/H_{c2}=0.93$, 1.035, and 1.14 for $L=4$, 5, and 6, respectively. Notice that for such a small hole in the disk the maximum number of L, i.e., $L=10$, is the same as for the disk case without a hole (see Fig. 4). The spatial distribution of the superconducting electron density $|\Psi|^2$ is depicted in the insets (a)–(c) of Fig. 14 for the multivortex state with $L=4$ at $H_0/H_{c2}=0.8$, $L=5$ at $H_0/H_{c2}=0.9$ and $L=6$ at $H_0/H_{c2}=1.0$, respectively. High (low) Cooper-pair density is given by dark (light) regions. Notice that there are always $L-1$ vortices in the superconducting material and one vortex appears in the hole, i.e., in the center of the ring.

The energy barriers for the transitions between the different L states are shown in Fig. 15 as a function of the applied magnetic field. By comparing this with the energy barriers for a disk with no hole, we see that the barrier heights and the transition fields are strongly different (see the inset of Fig. 4). Therefore we show in the insets of Fig. 15 the maximum height of the energy barrier $U_{\max}$ and the $L\leftrightarrow L+1$ transition field $H_{\rm tr}$ as a function of L for superconducting disks with no hole (squares) and with a hole of radius $R_i = 1.0\xi$ (circles), 2.0ξ (triangles), and 3.0ξ (stars). In all cases the height of the energy barrier decreases and the transition fields increase with increasing L. By comparing the situation with no hole and with a small hole with $R_i=1.0\xi$, we see that the barriers for $L\leqslant 1$ are higher for the disk with a hole with $R_i=1.0\xi$ than for $R_i=0.0\xi$, while they are smaller when $L>1$. Notice also that the value of the $L\rightarrow L+1$ transition field is sensitive to the presence of the hole with radius $R_i=1.0\xi$ for small L and insensitive for larger L. The reason is that for small $L>0$ such a central hole has always one vortex localized inside which favors certain vortex configurations above others, while for larger L in both cases only giant vortices appear with sizes larger than the hole size and the presence of the hole no longer matters. For larger holes the energy barrier decreases more slowly, because the free energy of the different L states shows a more parabolical type of behavior as a function of the magnetic field. The transition field has a much smaller dependence on the radius of the hole. Notice that the transition field for $R_i=3.0\xi$ is

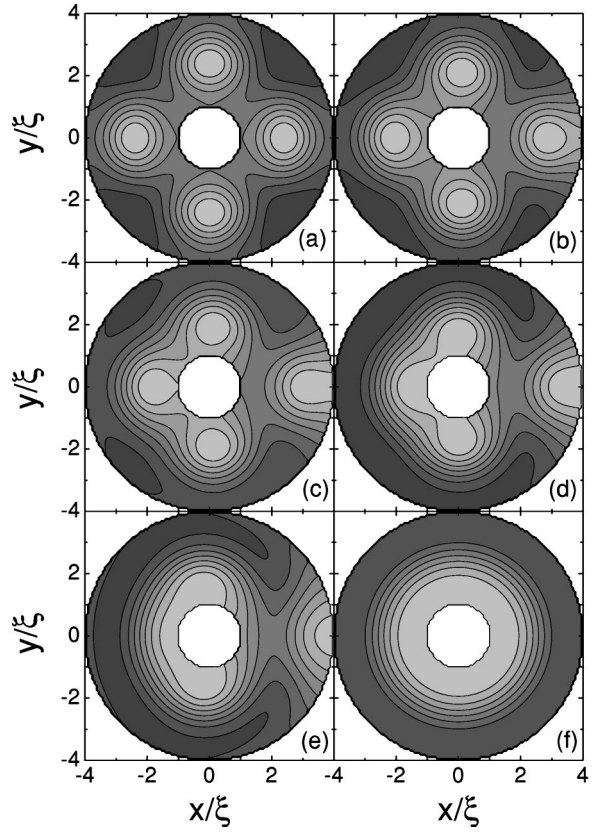

FIG. 16. The Cooper-pair density for the saddle point state transition between a multivortex state with $L=5$ and a giant vortex state with $L=4$ at $H_0/H_{c2}=0.83$ (a), 0.88 (b), 0.93 (c), 0.965 (d), 1.03 (e), and 1.06 (f). High Cooper-pair density is given by dark regions, low Cooper-pair density by light regions.

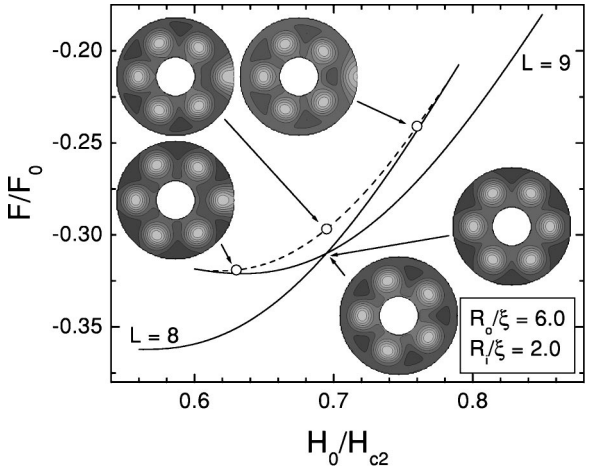

FIG. 17. The free energy of the multivortex states with $L=8$ and $L=9$ (solid curves) and the saddle point state (dashed curves) between these multivortex states for a superconducting ring with $R_0=6.0\xi$ and $R_i=2.0\xi$ as a function of the applied magnetic field. The lower insets show the spatial distribution of the superconducting electron density $|\Psi|^2$ at the transition field $H_0/H_{c2}=0.695$ for $L=8$ and $L=9$. The upper insets show the spatial distribution of the superconducting electron density $|\Psi|^2$ for the saddle point states indicated by the open circles, i.e., at $H_0/H_{c2}=0.63$ (a), 0.695 (b), and 0.76 (c). High Cooper-pair density is given by dark regions, low Cooper-pair density by light regions.

linear as a function of L for small holes and $L\leqslant 9$. This is in good agreement with the results in the narrow ring limit, where the transition between states with different vorticity L occurs when the enclosed flux ϕ equals $(L+1/2)\phi_0$.[37]

Next, we investigate the saddle point states in these superconducting rings. We make a distinction between different kinds of saddle point states; (i) between two giant vortex states, (ii) between a multivortex and a giant vortex state, (iii) between two multivortex states with the same vorticity in the hole and different vorticity in the superconducting material, and (iv) between two multivortex states with the same vorticity in the superconducting material but different vorticity in the hole. The first saddle point transition was already described for the case of small superconducting rings (see Figs. 11 and 12). Next, we study the saddle point state between a multivortex state with $L=5$ and a giant vortex state with $L=4$ for the previous considered ring with radius $R_0=4.0\xi$ and hole radius $R_i=1.0\xi$. Figures 16(a)–16(f) show the Cooper-pair density for these saddle point states at $H_0/H_{c2}=0.83$, 0.88, 0.93, 0.965 (i.e., the barrier maximum), 1.03 and 1.06, respectively. High (low) Cooper-pair density is given by dark (light) regions. For increasing field one vortex moves to the outer boundary, while the others move to the center of the ring where they create a giant vortex state. We remark that the giant vortex state is larger than the hole and therefore it is partially situated in the superconductor itself.

To study saddle point transitions between different multivortex states we have to increase the radius of the ring to favor the multivortex states. Therefore, we consider a ring with radius $R_0=6.0\xi$ and hole radius $R_i=2.0\xi$. Figure 17 shows the free energy of multivortex states with $L=8$ and $L=9$. In both cases 3 vortices are trapped in the hole. The lower insets show the spatial distribution of the superconducting electron density $|\Psi|^2$ at the transition field $H_0/H_{c2}=0.695$ for $L=8$ and $L=9$. It is clear that there are only 5 and 6 vortices in the superconducting material, respectively. The free energy of these multivortex states is shown by solid curves, while the saddle point energy between these states is given by the dashed curve. Notice further, that there is no transition from the multivortex states to the giant vortex states with $L=8$ and 9 as long as these states are stable. The spatial distribution of the superconducting electron density $|\Psi|^2$ for this saddle point state is depicted in the upper insets at the magnetic fields $H_0/H_{c2}=0.63$, 0.695 (the barrier maximum), and 0.76, respectively. For increasing field one vortex moves from the superconducting material to the outer boundary and hence the vorticity changes from $L=9$ to $L=8$. Notice that the vorticity of the interior boundary of the ring does not change.

The fourth type of saddle point state to discuss is the $L\rightarrow L+1$ transition between two multivortex states with the same vorticity in the superconducting material but with a different vorticity in the hole. For $R_0/\xi=4$ and $R_0/\xi=6$ we did not find such transitions regardless of the hole radius. This means that at least for these radii there is no transition

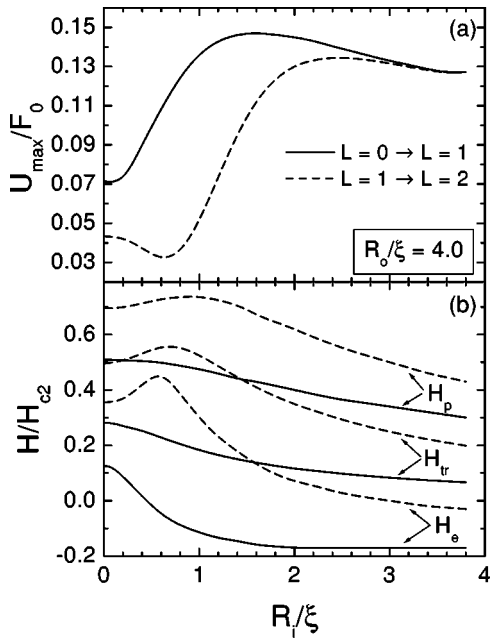

FIG. 18. (a) The maximum barrier height as a function of the hole radius R_i for a ring with radius $R_0=4.0\xi$ for the transition between the Meissner state and the $L=1$ state (solid curve) and the transition between the $L=1$ state and the $L=2$ state (dashed curve) and (b) the transition magnetic field H_{tr}, the expulsion magnetic field H_e and the penetration magnetic field H_p as a function of the hole radius R_i for the transition between the Meissner state and the $L=1$ state (solid curve) and the transition between the $L=1$ state and the $L=2$ state (dashed curve).

between such states which describes the motion of one vortex from the hole through the superconducting material towards the outer insulator.

Finally, we investigated the influence of the hole radius on the barrier for a fixed outer ring radius. Figure 18(a) shows the maximum barrier height, i.e., the barrier height at the thermodynamic equilibrium $L\rightarrow L+1$ transition, as a function of the hole radius R_i for a ring with radius $R_0=4.0\xi$ for the transition between the Meissner state and the $L=1$ state (solid curve) and for the transition between the $L=1$ and the $L=2$ state (dashed curve). For increasing hole radius, the barrier height of the first transition rapidly increases in the range $R_i=0.1\xi$ to $R_i=1.5\xi$ and decreases slowly afterwards. For a superconducting disk with radius $R_0=4.0\xi$ with a hole in the center with radius $R_i=1.5\xi$ the maximum barrier height for the $0\rightarrow 1$ transition is twice as large as for a superconducting disk without a hole. The barrier height of the second transition first decreases, then rapidly increases in the range $R_i=0.6\xi$ to $R_i=2.5\xi$ and then slowly decreases again. In this case the maximum barrier height for a superconducting disk with a hole with radius $R_i=2.5\xi$ is three times as large as for a superconducting disk without a hole. Hence, changing the hole radius strongly influences the maximum height of the barrier. In Fig. 18(b) we plot the characteristic magnetic fields of the barrier as a function of the hole radius, i.e., the transition magnetic field $H_{\rm tr}$, the expulsion magnetic field H_e, and the penetration magnetic field H_p, for the $0\rightarrow 1$ transition by solid curves and for the $1\rightarrow 2$ transition by the dashed curve. For the $0\rightarrow 1$ transition the characteristic magnetic fields decrease with increasing hole radius. For the $1\rightarrow 2$ transition the characteristic magnetic fields first increase to a maximum and then decrease. This behavior was described and explained in our previous paper (see, e.g., Fig. 17 of Ref. 14). Notice that the position of the minimum in $U_{\rm max}$ coincides with the position of the maximum in H_{tr}.

V. CONCLUSIONS

We studied the saddle points for transitions between different vortex states for thin superconducting disks and rings. A distinction was made between small systems where the confinement effects dominate and larger systems where multivortices can nucleate for certain magnetic fields. At the entrance of the vortex into the superconducting material the superconducting density becomes zero at a certain point at the edge of the disk or ring. Such a zero in the order parameter acts as a phase slip center which allows the vorticity to increase with one unit. For the case of the ring the vortex may enter (or exit) the superconducting material from the inner boundary or from the outer boundary of the ring.

We studied the transition between two giant vortex states with different vorticity L. One vortex moves through the superconducting material to the center of the disk or to the hole. During the transition the position of this vortex in the superconductor can be determined very precisely, because the Cooper-pair density is exactly zero in the center of this vortex. The transition between a multivortex state and a giant vortex state with different vorticity L is also described. One vortex leaves (enters) the superconductor while the other vortices move towards (away from) the center of the disk. For large enough disk/ring radii, we calculated the transition between two multivortex states. We found such transitions between two multivortex states with different vorticity L in the superconductor but with the same vorticity in the center/hole. One vortex enters/leaves the superconductor while the other vortices rearrange themselves. Transitions between different multivortex states with the same vorticity in the superconducting material but different vorticity in the hole were not found for the considered ring configurations, which means that transitions between such states do not occur in these particular cases.

The maximum height of the energy barrier always decreases for increasing L. Near the maximum, the barrier height decreases linearly and its slope at the left side ($H\lesssim H_{\rm max}$) of the maximum is not equal to the slope at the right side ($H\gtrsim H_{\rm max}$). The barrier shape and height strongly depend on the radius of the hole in the center of the disk.

ACKNOWLEDGMENTS

This work was supported by the Flemish Science Foundation (FWO-Vl), the ''Onderzoeksraad van de Universiteit Antwerpen,'' the ''Interuniversity Poles of Attraction Program - Belgian State, Prime Minister's Office - Federal Office for Scientific, Technical and Cultural Affairs,'' and the European ESF-Vortex Matter. Discussions with S. Yampolskii are gratefully acknowledged.

*Electronic address: peeters@uia.ua.ac.be
†Permanent address: Institute of Theoretical and Applied Mechanics, Russian Academy of Sciences, Novosibirsk 630090, Russia.

[1] O. Buisson, P. Gandit, R. Rammel, Y. Y. Wang, and B. Pannetier, Phys. Lett. A **150**, 36 (1990).
[2] A. K. Geim, I. V. Grigorieva, S. V. Dubonos, J. G. S. Lok, J. C. Maan, A. E. Filippov, and F. M. Peeters, Nature (London) **390**, 256 (1997).
[3] P. S. Deo, V. A. Schweigert, F. M. Peeters, and A. K. Geim, Phys. Rev. Lett. **79**, 4653 (1997).
[4] R. Benoist and W. Zwerger, Z. Phys. B: Condens. Matter **103**, 377 (1997).
[5] V. A. Schweigert and F. M. Peeters, Phys. Rev. B **57**, 13 817 (1998).
[6] V. A. Schweigert, F. M. Peeters, and P. S. Deo, Phys. Rev. Lett. **81**, 2783 (1998).
[7] J. J. Palacios, Physica B **256-258**, 610 (1998); Phys. Rev. B **58**, R5948 (1998).
[8] V. M. Fomin, V. R. Misko, J. T. Devreese, and V. V. Moshchalkov, Phys. Rev. B **58**, 11 703 (1998).
[9] E. Akkermans and K. Mallick, J. Phys. A **32**, 7133 (1999).
[10] P. S. Deo, F. M. Peeters, and V. A. Schweigert, Superlattices Microstruct. **25**, 1195 (1999).
[11] V. Bruyndoncx, J. G. Rodrogo, T. Puig, L. Van Look, and V. Moshchalkov, Phys. Rev. B **60**, 4285 (1999).
[12] J. Berger and J. Rubinstein, Phys. Rev. Lett. **75**, 320 (1995); Phys. Rev. B **56**, 5124 (1997); **59**, 8896 (1999).
[13] V. Bruyndoncx, L. Van Look, M. Verschuere, and V. V. Moshchalkov, Phys. Rev. B **60**, 10 468 (1999).
[14] B. J. Baelus, F. M. Peeters, and V. A. Schweigert, Phys. Rev. B **61**, 9734 (2000).
[15] F. M. Peeters, V. A. Schweigert, B. J. Baelus, and P. S. Deo, Physica C **332**, 255 (2000).
[16] H. J. Fink, Phys. Rev. **151**, 219 (1966).
[17] C. P. Bean and J. B. Livingston, Phys. Rev. Lett. **12**, 14 (1964).
[18] V. P. Galaiko, Zh. Éksp. Teor. Fiz. **50**, 1322 (1966) [Sov. Phys. JETP **23**, 878 (1966)]; B. V. Petukhov and V. R. Chechetkin, *ibid.* **65**, 1653 (1973) [**38**, 827 (1974)].
[19] A. L. Fetter, Phys. Rev. B **22**, 1200 (1980).
[20] V. G. Kogan, Phys. Rev. B **49**, 15 874 (1980); A. V. Kuznetsov, D. V. Eremenko, and V. N. Trofimov, *ibid.* **59**, 1507 (1999).
[21] M. V. Indenbom, H. Kronmüller, T. W. Li, P. H. Kes, and A. A. Menovsky, Physica C **222**, 203 (1994); Th. Schuster, M. V. Indenbom, H. Kuhn, E. H. Brandt, and M. Konczykowski, Phys. Rev. Lett. **73**, 1424 (1994); E. Zeldov, A. I. Larkin, V. B. Geshkenbein, M. Konczykowski, D. Majer, B. Khaykovich, V. M. Vinokur, and H. Schtrikman, *ibid.* **73**, 1428 (1994).
[22] J. S. Langer and V. Ambegaokar, Phys. Rev. **164**, 498 (1967); X. Zhang and J. C. Price, Phys. Rev. B **55**, 3128 (1997).
[23] P. Singha Deo, V. A. Schweigert, and F. M. Peeters, Phys. Rev. B **59**, 6039 (1999).
[24] A. K. Geim, S. V. Dubonos, J. G. S. Lok, M. Henini, and J. C. Maan, Nature (London) **396**, 144 (1998).
[25] E. Akkermans, D. M. Gangardt, and K. Mallick, Phys. Rev. B **63**, 064523 (2001).
[26] J. J. Palacios, Phys. Rev. Lett. **84**, 1796 (2000).
[27] V. A. Schweigert and F. M. Peeters, Physica C **332**, 426 (2000).
[28] V. V. Moshchalkov, X. G. Qiu, and V. Bruyndoncx, Phys. Rev. B **55**, 11 793 (1997).
[29] G. F. Zharkov, cond-mat/0009043 (unpublished).
[30] A. K. Geim, S. V. Dubonos, I. V. Grigorieva, K. S. Novoselov, F. M. Peeters, and V. A. Schweigert, Nature (London) **407**, 55 (2000).
[31] V. A. Schweigert and F. M. Peeters, Phys. Rev. Lett. **83**, 2409 (1999).
[32] A. Bezryadin, A. Buzdin, and B. Pannetier, Phys. Rev. B **51**, 3718 (1995).
[33] E. M. Horane, J. J. Castro, G. C. Buscaglia, and A. Lopez, Phys. Rev. B **53**, 9296 (1995).
[34] S. V. Yampolskii and F. M. Peeters, Phys. Rev. B **62**, 9663 (2000).
[35] M. Zalalutdinov, H. Fujioka, Y. Hashimoto, S. Katsumoto, and Y. Iye, J. Phys. Soc. Jpn. **68**, 2872 (1999).
[36] A. K. Geim, S. V. Dubonos, J. J. Palacios, I. V. Grigorieva, M. Henini, and J. J. Schermer, Phys. Rev. Lett. **85**, 1528 (2000).
[37] See, e.g., M. Thinkham, *Introduction to Superconductivity* (McGraw-Hill, London, 1975).